Climate Dynamics (2019) 52:15–27
https://doi.org/10.1007/s00382-018-4125-3

Impacts of model spatial resolution on the vertical structure of convection in the tropics

Hien Xuan Bui[1] · Jia-Yuh Yu[1] · Chia Chou[2,3]

Received: 20 June 2017 / Accepted: 29 December 2017 / Published online: 22 February 2018

Abstract
This study examined the impacts of model horizontal resolution on vertical structures of convection in the tropics by performing sensitivity experiments with the NCAR CESM1. It was found that contributions to the total precipitation between top-heavy and bottom-heavy convection are different among various resolutions. A coarser resolution tends to produce a greater contribution from top-heavy convection and, as a result, stronger precipitation in the western Pacific ITCZ; while there is less contribution from bottom-heavy convection and weaker precipitation in the eastern Pacific ITCZ. In the western Pacific ITCZ, where the convection is dominated by a top-heavy structure, the stronger precipitation in coarser resolution experiments is due to changes in temperature and moisture profiles associated with a warmer environment (i.e., thermodynamical effect). In the eastern Pacific ITCZ, where the convection is dictated by a bottom-heavy structure, the stronger precipitation in finer resolution experiments comes from changes in convection structure (i.e., dynamic effect) which favors a greater contribution of bottom-heavy convection as the model resolution goes higher. The moisture budget analysis further suggested that the very different behavior in precipitation tendencies in response to model resolution changes between the western and eastern Pacific ITCZs are determined mainly by changes in convective structure rather than changes in convective strength. This study pointed out the importance of model spatial resolution in reproducing a reasonable contribution to the total precipitation between top-heavy and bottom-heavy structure of convection in the tropical Pacific ITCZs.

1 Introduction

The core of tropical dynamics involves strong interaction between cumulus convection and large-scale perturbations. A reasonable representation of the collective effect of subgrid scale cumulus convection process in a large-scale atmospheric model is the key to produce a successful simulation of the time-mean tropical circulation and its associated variability. The cumulus convection can be in general divided into two major categories with different intensity of precipitation, namely, deep convection and shallow convection. In addition, congestus clouds are also an important category whose tops stop at slightly above the freezing level (Johnson et al. 1999).

To illustrate the feedback of convective processes on large-scale flows, Yanai et al. (1973) proposed the diagnosis of apparent heat source (Q_1) and apparent moisture sink (Q_2). Diabatic heating in the atmosphere is a combined consequence of radiation heating from both shortwave and longwave, and latent heating from phases changes associated with convection. Vertical profiles of diabatic heating with global coverages have been estimated from satellite retrievals (Tao et al. 2006). However differences among retrieval algorithms could lead to discrepancies in the vertical structures. Besides, many studies have also employed the reanalysis data to examine the horizontal distributions, amplitude and vertical structure of diabatic heating (Nigam et al. 2000; Chan and Nigam 2009; Hagos et al. 2010; Ling and Zhang 2013). A surprising result in these studies is that the tropical heating profiles among the reanalysis were quite diverse. Many studies, such as Schumacher et al. (2007),

Electronic supplementary material The online version of this article (https://doi.org/10.1007/s00382-018-4125-3) contains supplementary material, which is available to authorized users.

✉ Jia-Yuh Yu
jiayuh@atm.ncu.edu.tw

[1] Department of Atmospheric Sciences, National Central University, Taoyuan City, Taiwan

[2] Research Center for Environmental Changes, Academia Sinica, Taipei, Taiwan

[3] Department of Atmospheric Sciences, National Taiwan University, Taipei, Taiwan

Takayabu et al. (2010), Hagos et al. (2010) have discussed the double peak structure in the vertical heating profiles. The upper peak is coming from the stratiform and deep convection while the lower peak is coming from the shallow and congestus clouds, which is also in agreement with recent study of Johnson et al. (2016).

One of the common biases in modeled tropical precipitation is the underestimation of heavy precipitation events due to the coarse spatial resolution of the model (Gregory et al. 1997; Stephens et al. 2010). For example, Deser et al. (2006) compared the mean precipitation simulations for a version of the Community Atmospheric Model (CAM3) using T42 and T85 resolutions, respectively. They found that spatial pattern of precipitation in low-resolution simulation shows significant quantitative errors, even though the major features are consistent with observations. By examining the mean summer precipitation over the tropical ocean, Hack et al. (2006) showed a locally significant meridional redistribution of precipitation as a function of spatial resolution.

Climate models have been extensively used over the past two decades to project future climate changes under the anthropogenic greenhouse warming. Although most of the climate models used in CMIP5 have increased spatial resolution compared to those used in CMIP3, some still keep relatively low resolution, e.g., CMSS-CESM (3.75° × 3.75°), HadCM3 (3.75° × 2.5°), FGOALS-g2 and MIROC-ESM (2.8125° × 2.8125°), GFDL-CM2.1 (2.5° × 2°) and GISS-E2-H (2° × 2.5°). It is thus worth knowing how the model's spatial resolution impacts the vertical structure of convection in the Tropics because the efficiency of moist static energy export by cumulus convection depends largely on the structure of convection (Back and Bretherton 2006; Bui et al. 2016).

Differences in physical parameterization and model resolution are two major factors from which most of the biases in the contemporary climate models come. In this study, we examine the impacts of model spatial resolution on vertical structures of convection in climate, focusing on how the contribution between top-heavy and bottom-heavy convection might change in various model resolutions. We run the Community Atmospheric Model (CAM) version 5 with four spatial resolutions: 400, 200, 100 and 50 km to cover the spectra of grid sizes of contemporary climate models. Section 2 presents an overview of the atmospheric model and the design of sensitivity experiments. A brief introduction of satellite and field campaign datasets is also presented in this section. Section 3 describes the diabatic heat source and moisture sink as well as the bin method used to identify top-heavy and bottom-heavy convection cases. Major results are presented and discussed in detail in Sect. 4. Section 5 utilizes the moisture budget analysis to examine the dynamic and thermodynamic feedbacks on precipitation. A summary and discussion is given in Sect. 6.

2 Design of sensitivity experiments

2.1 The atmospheric model

The atmospheric model used in this study is the Community Atmospheric Model version 5 (CAM5) (Neale et al. 2010), which is the atmospheric component of the National Center for Atmospheric Research (NCAR) Community Earth System Model (CESM), with a finite-volume dynamical core (Lin 2004) and an integration time step of 1800 s (30 min). In CAM5, the default number of vertical levels is 30, with four additional layers below 700 hPa compared to the CAM4 due to a new parameterization of the boundary layer (Park and Bretherton 2009). The deep convection scheme (Zhang and McFarlane 1995) has been improved, including the effects of deep convection in the momentum equation (Richter and Rasch 2008) and the interaction between convective air with its environment (Neale et al. 2008). The Park and Bretherton (2009) shallow convection scheme (also known as the UWShCu scheme), in which the fundamental frame work and closure assumption are based on Bretherton et al. (2004), is used to parameterize the collective effect of shallow cumulus convection. The mass flux at the cloud base is determined by the ratio between convective inhibition (CIN) and turbulent kinetic energy (TKE) which is provided by the boundary layer scheme (Bretherton and Park 2009) to ensure the interaction between boundary layer and cumulus convection.

In the UWShCu scheme, the entrainment and detrainment processes are determined by buoyancy sorting algorithm from Kain and Fritsch (1990). There is no limitation for the cloud height, however, because the deep convection scheme is performed first in CAM5, which provides a tendency to stabilize the atmosphere, the cloud top height simulated by shallow scheme is thus internally limited (Neale et al. 2010). For the microphysics process, a simple assumption is applied in which the cloud condensation amount larger than 1g/kg is removed from the updraft as precipitation and the remainder is detrained in to the environment. As mentioned in Neale et al. (2010), the current scheme also neglects the radiation effect and evaporation of convective precipitation within the convective updraft.

2.2 The sensitivity experiments

The CAM5 simulations with a prescribed SST of Year 1850 are tested at four different spatial resolutions from 4°, 2°, 1° to 0.5°, corresponding to a grid spacing of about 400, 200, 100 and 50 km, respectively, in the equatorial region. All the simulations are run for 12 years with daily outputs, but only the outputs from the last 10 years are used for analysis.

Besides the changes in the spatial resolution, there are slight differences in some parameters between the sensitivity experiments as these parameters are made functions of spatial resolution in CAM5 to ensure energy balance at the top of atmosphere (Hack et al. 2006; Boyle and Klein 2010). The most significant one is the value of penetrative updraft entrainment efficiency (r_{pen}) in the shallow convection scheme between 2° spatial resolution run and the others which are 5 and 10, respectively. In addition, there is also a small change in the value of minimum relative humidity for low clouds (0.8975 for 1° and 0.8875 for 2°). To ensure consistency, we carried out some sensitivity tests and found that these differences in practice do not alter the results and conclusions of this study (not shown).

2.3 Satellite and field campaign datasets

To validate the model's performance in simulating precipitation climatology, we use the satellite derived precipitation data from the Tropical Rainfall Measuring Mission (TRMM) during the period 1998–2007. The original spatial resolution is 0.25° but we made an interpolation to different resolutions to be consistent with the CESM outputs.

For the vertical profiles of convection, some field campaign datasets are also employed for comparison purpose (Table 1). These include the Tropical Ocean Global Atmosphere Coupled Ocean–Atmosphere Response Experiment (TOGA COARE), the South China Sea Monsoon Experiment (SCSMEX), the Kwajelin Experiment (KWAJEX), the Tropical Warm Pool International Cloud Experiment (TWP ICE), and the ARM MJO Investigation Experiment (AMIE). All the 6-hourly data with a vertical grid at 25 hPa intervals from 1000 to 100 hPa are analyzed.

3 Method of analysis

3.1 Apparent heat source (Q_1) and moisture sink (Q_2)

Apparent heat source (Q_1) and moisture sink (Q_2) were estimated using gridpoint temperature, moisture and wind (Yanai and Johnson 1993), which can be written as:

$$Q_1 \equiv \frac{\partial \overline{s}}{\partial t} + \overline{\mathbf{v}} \cdot \nabla \overline{s} + \overline{\omega}\frac{\partial \overline{s}}{\partial p} = Q_R + L(\overline{c} - \overline{e}) - \nabla \cdot \overline{s'\mathbf{v}'} - \frac{\partial \overline{s'\omega'}}{\partial p} \quad (1)$$

and

$$Q_2 \equiv -L\left(\frac{\partial \overline{q}}{\partial t} + \overline{\mathbf{v}} \cdot \nabla \overline{q} + \overline{\omega}\frac{\partial \overline{q}}{\partial p}\right) = L(\overline{c} - \overline{e}) + L\nabla \cdot \overline{q'\mathbf{v}'} + L\frac{\partial \overline{q'\omega'}}{\partial p} \quad (2)$$

where Q_R is the heating rate due to radiation, c is the rate of condensation per unit mass of air, e is the rate of re-evaporation of the suspending cloud water and falling rain drop per unit mass, $s = C_pT + gz$ is the dry static energy, T is temperature, ω is pressure velocity, and q is the mixing ratio of water vapor. The horizontal averages are denoted by $\overline{(\,)}$ and deviations from the horizontal averages are denoted by primes.

Apparent heat source (Q_1) is the heating resulted from the diabatic cumulus convection processes (including net condensation and convergence of eddy heat flux) in the atmosphere. Moisture sink (Q_2) is associated with the moisture loss due to net condensation and divergence of eddy moisture transport (Yanai et al. 1973). The advantage of using these two variables is that they provide the relationship and interaction between the cumulus convection and the large-scale environment.

3.2 The dependence of convective vertical structure on precipitation rate

Instead of using the direct precipitation outputs from the model convection (precipitation) schemes, we identify the top-heavy and bottom-heavy convection cases based on different precipitation intensity bins and then examine how model resolution change affects the structure of convection. The motivation behind this design was to highlight the relationship between the vertical structure of convection and precipitation intensity in a climatological (or statistical) sense (Bui et al. 2016). Even though there are many studies focusing on the time-mean rainfall patterns [Neelin (2007) and reference therein], investigation on changes of precipitation characteristics is needed, especially when the intensity and frequency of both heavy and light precipitation events

Table 1 List of the field campaign datasets used in this study

Field campaign	Location	Period	References
TOGA COARE	10°S–10°N, 140°E–180	1 Nov 1992–28 Feb 1993	Webster and Lukas (1992)
SCSMEX	Southern China Sea	5 May–20 Jun 1998	Lau et al. (2000)
KWAJEX	7–10°N, 166–169°E	24 Jul–14 Sep 1999	Sobel et al. (2004)
TWP ICE	Darwin Island	17 Jan–12 Feb 2006	Xie et al. (2010)
AMIE (TRMM)	Gan Island, Indian Ocean	13 Nov–13 Dec 2011	Stokes and Schwartz (1994)

could possibly change under global warming (Chen et al. 2016).

In this study, we practically identify the different convection structures based on regime sorting performed in the large-scale conditions and convection properties (Takayabu et al. 2010). The data are sorted and binned according to precipitation intensity (Hagos et al. 2010) with a total of 100 bins (i.e., each bin contains 1% of the total sampled precipitation events), similar to the percentile ranks. In our analysis, a precipitation event is defined as the precipitation rate greater than 0.1 mm day^{-1} as in previous studies (Sun et al. 2007; Chou et al. 2012). The first few bins represent light precipitation events, which are presumably dominated by shallow bottom-heavy convection; while the last few bins denote heavy precipitation events, in which both top-heavy and bottom-heavy convection often coexist, in agreement with the results from Hagos et al. (2010). Once obtaining the precipitation bins, we then look at the corresponding vertical profiles.

To extract the convection contribution from the radiative cooling and others effects, we subtract the 1st bin from the very light rain and the 91st bin from the very heavy rain with the assumption that radiation cooling profile does not change too much among precipitation bins. In the heavy-rain regime (rainfall events within 91–100th percentile bins), as the cloud tops are located at various levels, strong cancellations between heating and cooling occur within the convective column, resulting in a relatively uniform radiative profile. Thus, subtracting the 91st bin, to a large extent, may remove the effect associated with radiation. In the light-rain regime (rainfall events within 1–10th percentile bins), the radiative profile is in nature uniform, subtracting the 1st bin not only removes the effect associated with radiation, it also excludes the background climatology of light-rain regime dominated by strong subsidence. This allows us to highlight the convection structure changes associated with shallow cumulus. As in Chen et al. (2016), we also normalized the original profile through dividing it by a normalization factor that represents the magnitude of the profile (i.e., the value x in each level p by dividing by $[\sum_{P_S}^{P_T} x(p)^2]^{1/2}$ with P_T and P_S being 100 and 1000 hPa, respectively) to focus only on the vertical structure.

4 Impacts of spatial resolution on simulations of tropical climate

4.1 Contrast between heavy-rain and light-rain regimes

To assess how the model spatial resolution affects the vertical structure of convection, the vertical distributions of Q_1 and Q_2 averaged over the first 10 bins between 20°S and 20°N were first examined (Fig. 1a, b). There is a maximum of Q_1 at 900 hPa accompanied by a minimum at 800 hPa for all four experiments (Fig. 1a), indicating that light rain events are generally associated with bottom-heavy convection. We note that the above Q_1 maximum should come from the latent heating of net moisture condensation and the Q_1 minimum is a result of the re-evaporation cooling due to detrainment at the top of shallow convection (see the pressure velocity field in Fig. 1c for comparison). The above feature is consistent with the Q_2 profile, i.e., a maximum moisture sink at 900 hPa and a moisture source at 800 hPa. The Q_1 and Q_2 profiles also correspond well with ascending motions below 850 hPa, i.e., a strong low-level convergence (upward motion) near the surface and a divergence (downward motion) maximum at about 850 hPa (Fig. 1c, d) except for the coarsest resolution experiment. For the temperature field, a warming peak is found near the surface and a maximum cooling at 850 hPa (Fig. 1e). The divergence and moisture fields (Fig. 1d, f) are controlled by convection, which generally show opposite phases with the pressure field (Fig. 1c). These results demonstrate typical dynamic and thermodynamic profiles of bottom-heavy convection, and its role in vertically redistributing the moisture and temperature fields below 800 hPa.

We next compare results between the experiments with different spatial resolutions. In the vertical structure of kinematic fields, it is clear that the coarsest resolution experiment (blue curves in Fig. 1c, d) behaves differently from the finer resolution ones. It may be due to the fact that parts of shallow convection with smaller scales are not fully represented in the coarsest resolution experiment, so the background subsidence tends to dominate the dynamic fields. In general, the strength of bottom-heavy convection does not have a clear relationship with the spatial resolution without the co-existence of top-heavy convection. We also find that there is a local peak of ascending motion at around 300 hPa for finer resolution runs (see Fig. 1c), even though no corresponding changes of thermodynamic profiles due to the much drier upper-level atmospheric environment for the first 10 precipitation bins. The thermodynamic structures of bottom-heavy convection (e.g., Q_1, Q_2, T and q profiles) show less dependence on the spatial resolution compared with the kinematic structures (e.g., omega and divergence profiles).

Likewise, Fig. 2 shows the same dynamic and thermodynamic fields but averaged over the last 10 bins to assess the spatial resolution effect on heavy precipitation events. As shown, all four experiments exhibit 2 peaks, one in the lower troposphere and the other in the upper troposphere, a clear evidence of the coexistence of top-heavy and bottom-heavy convection. Figure 2a shows the structure of Q_1 with double peaks at around 800 and 350 hPa, corresponding to the release of latent heat from top-heavy and bottom-heavy

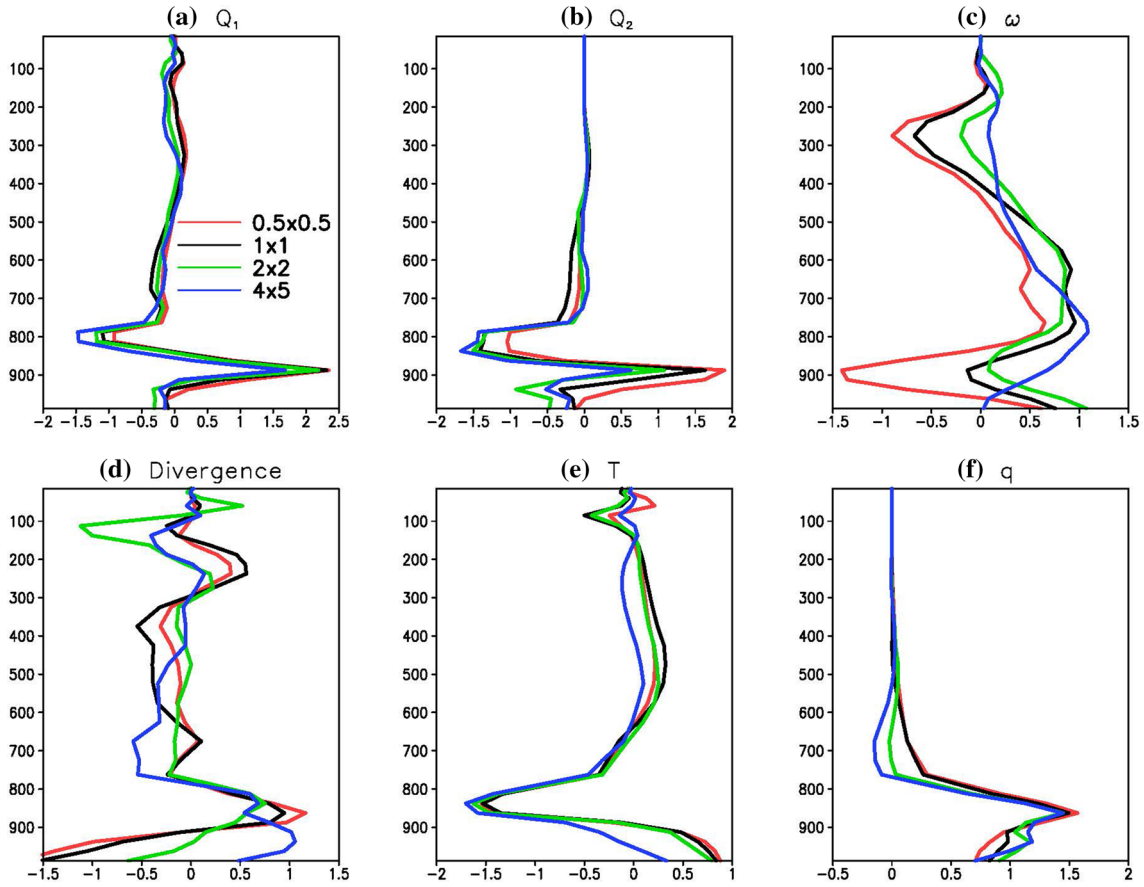

Fig. 1 The normalized vertical structures of **a** Q_1, **b** Q_2, **c** ω, **d** divergence, **e** temperature and **f** specific humidity averaged over 1–10th bins

convection, respectively. Q_2 shows a very similar profile to Q_1, with two peaks at around 800 hPa and 400 hPa (Fig. 2b). The ascending motion shows two maxima at around 800 and 300 hPa (Fig. 2c), consistent with the divergence field shown in Fig. 2d. Unlike what happens in light-rain regime (Fig. 1e), the temperature structure in heavy-rain regime shows a weak cooling near the surface and around 600 hPa for all experiments (Fig. 2e), possibly due to re-evaporation cooling of falling raindrops. The significant upper warming above 400 hPa is dominated by the moist adiabatic heating, as discussed in Holloway and Neelin (2007). The moisture field also shows two peaks around 700 and 400 hPa (Fig. 2f).

As the spatial resolution becomes finer, the lower peak in both dynamics and thermodynamics fields becomes larger, while the corresponding upper peak appears to have a reverse tendency. This implies that a change in the contribution between top-heavy and bottom-heavy convection occurs when the model spatial resolution varies. In short, a greater contribution of bottom-heavy convection and a less contribution of top-heavy convection are found in the finer resolution experiments, which is in agreement with the previous study of Boyle and Klein (2010).

To see whether the above features exist in observations, we analyze the data from several field observations (Table 1). Note that these data were gathered in a limited area and time period in the Tropics when a particular weather system occurred. Because sampling sizes of these datasets are small, they inclined to exhibit features of heavy precipitation events. Therefore, we only compare these profiles with Fig. 2. Figure 3 depicts the vertical structures of Q_1 and Q_2 from the field observations. Both Q_1 and Q_2 profiles exhibit a somewhat double peak structure as in the finer resolution experiments of CESM (Fig. 2a, b), except that the maximum levels of heating and moisture sink (at around 450 hPa and 500 hPa, respectively) are slightly lower in observations (Fig. 3a, b). This is in agreement with the results from Yanai and Johnson (1993), in which the differences in the peaks of Q_1 and Q_2 suggests the presence of eddy vertical transport of moist static energy associated with cumulus convection. These observational results show a clear evidence of the coexistence of top-heavy and bottom-heavy convection in presence of heavy precipitation events, and the finer resolution experiments ($1° \times 1°$ and $0.5° \times 0.5°$) are more capable than the lower ones ($2° \times 2°$ and $4° \times 5°$)

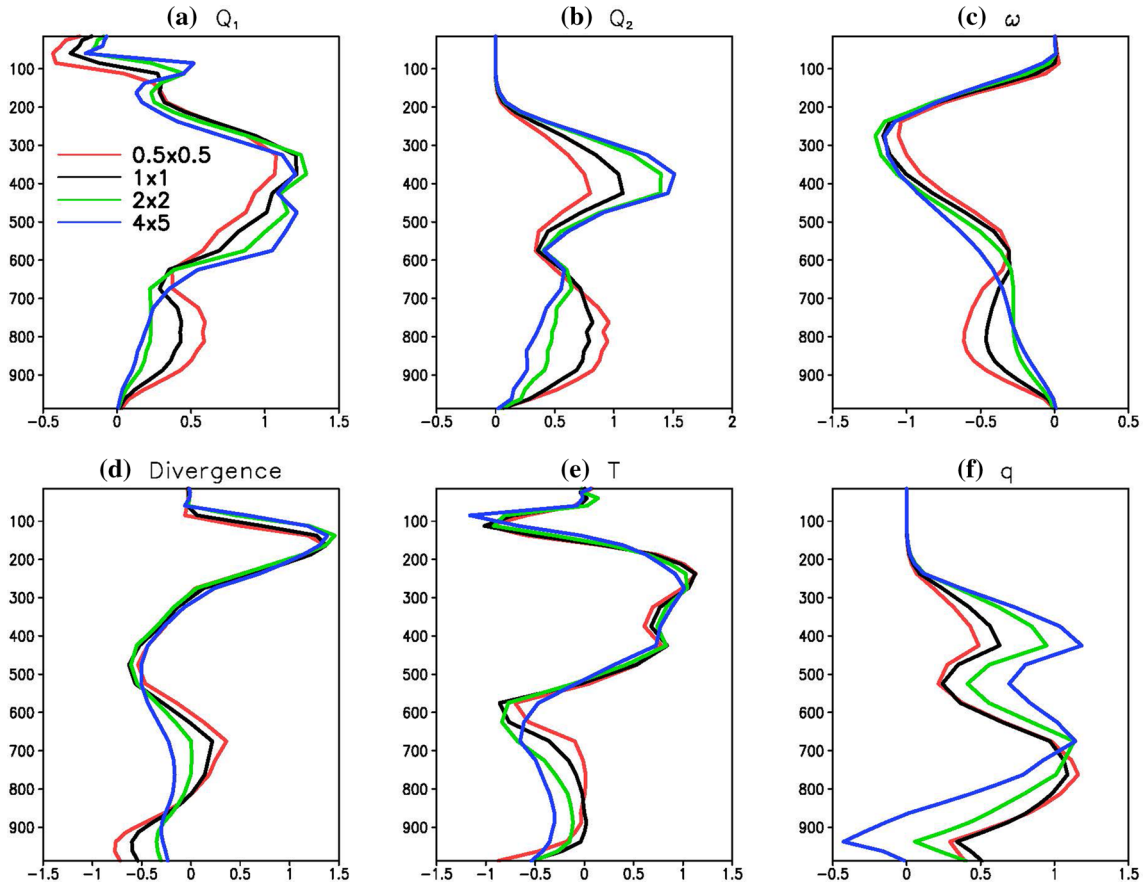

Fig. 2 As in Fig. 1 but averaged over 91–100th bins

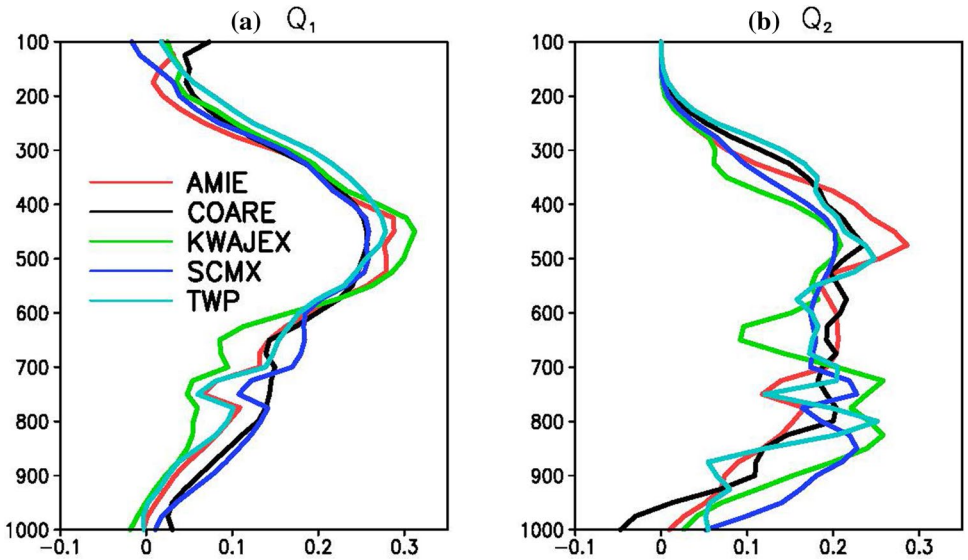

Fig. 3 The normalized vertical structures of **a** Q_1, **b** Q_2 from field campaign datasets

in reproducing the observed contribution of top-heavy and bottom-heavy convection (see Fig. 2a, b for comparison).

Figure 4a shows the zonal distribution of pressure velocity at 500 hPa averaged over 0–10°N for the four experiments. The coarser resolution experiment produces stronger upward motion in the western Pacific, but weaker upward motion in the eastern Pacific ITCZ. For comparison, the climatology of temperature and specific humidity are

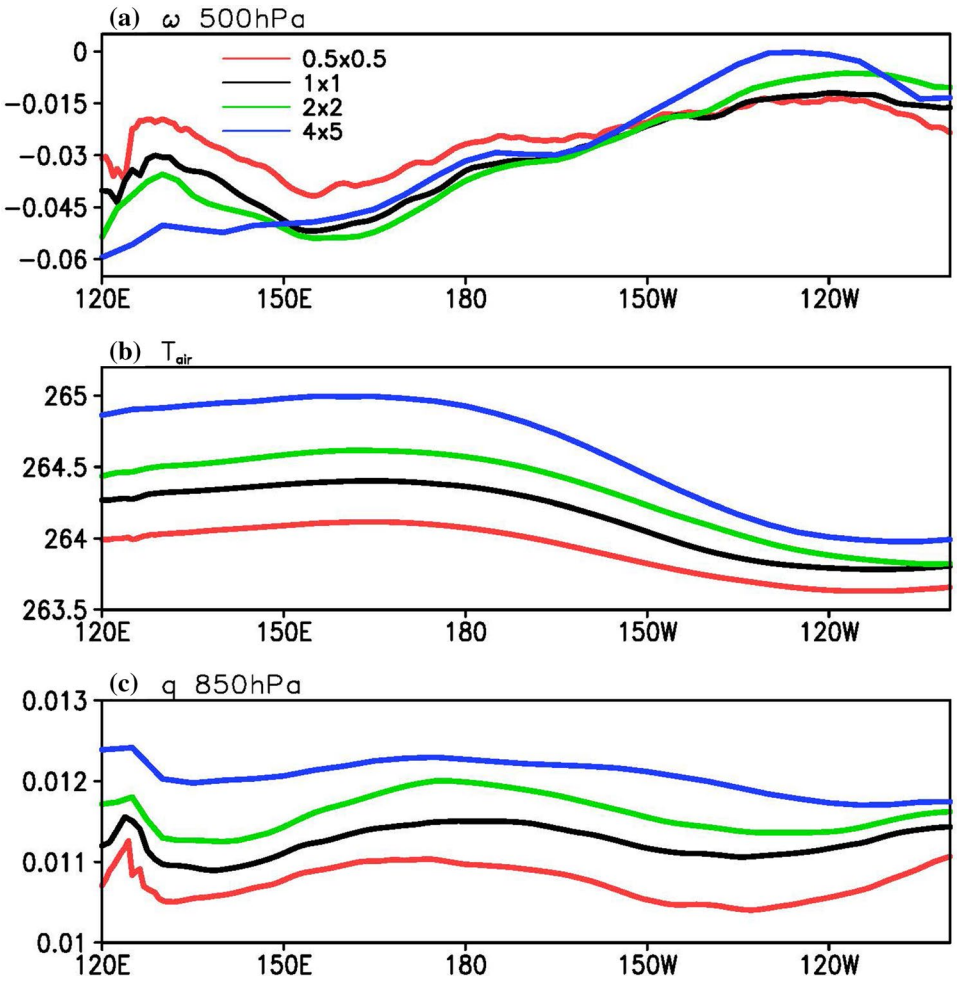

Fig. 4 The meridional averages (0–10°N) of **a** omega at 500 hPa (unit is Pa s^{-1}), **b** mean tropospheric temperature from 850–200 hPa (unit is K) and **c** specific humidity at 850 hPa (unit is kg kg^{-1}) for four different spatial resolutions

also shown in Fig. 4b, c, respectively. In general, a warmer and moister troposphere tends to occur in the coarser resolution experiments. From the entire tropical Pacific point of view, the corresponding model precipitation also shows a consistent result, i.e., a warmer and moister troposphere tends to generate a greater amount of the total tropical precipitation (Fig. 5). In other words, the thermodynamic effect is a dominant factor in determining the magnitude of tropical precipitation. This is very similar to tropical precipitation changes found in global-warming simulations (e.g., Chou and Neelin 2004; Held and Soden 2006; Chou et al. 2009).

From the regional point of view, the dependence of tropical precipitation on model resolution, however, differs significantly between the eastern and western Pacific ITCZs, as shown in Fig. 5. In the western Pacific warm pool, the coarser resolution experiment exhibits a stronger magnitude of precipitation; while in the eastern Pacific ITCZ, the coarser resolution experiment generates a weaker magnitude of precipitation. In the following section, we will provide a detailed analysis to explain why the magnitude of precipitation in response to model resolution changes is so different between the eastern and western Pacific ITCZs.

4.2 Contrast between western and eastern Pacific ITCZs

The dependence of regional precipitation on model spatial resolution provides an opportunity to identify changes in convective structure and precipitation between the western and eastern Pacific ITCZs. Following Bui et al. (2016), two target domains over the western and the eastern Pacific ITCZs are selected as shown by the rectangular boxes in Fig. 5. These domains are located within heavy convective regions, with precipitation rate all greater than 4 mm day^{-1}. Figure 6a shows the area means of precipitation over these two domains. As the resolution decreases, the precipitation intensity increases over the western Pacific ITCZ but decreases in the eastern Pacific ITCZs, consistent with the results shown in Fig. 5. If we consider only the heavy-rain regime (91–100th bins), the dependence of precipitation on the model spatial resolution exhibits a similar trend (Fig. 6b) except that the increase of precipitation with the decrease (increase) of the spatial resolution in the western (eastern) Pacific ITCZ is slower (faster) than the total precipitation shown in Fig. 6a. The greater sensitivity of precipitation

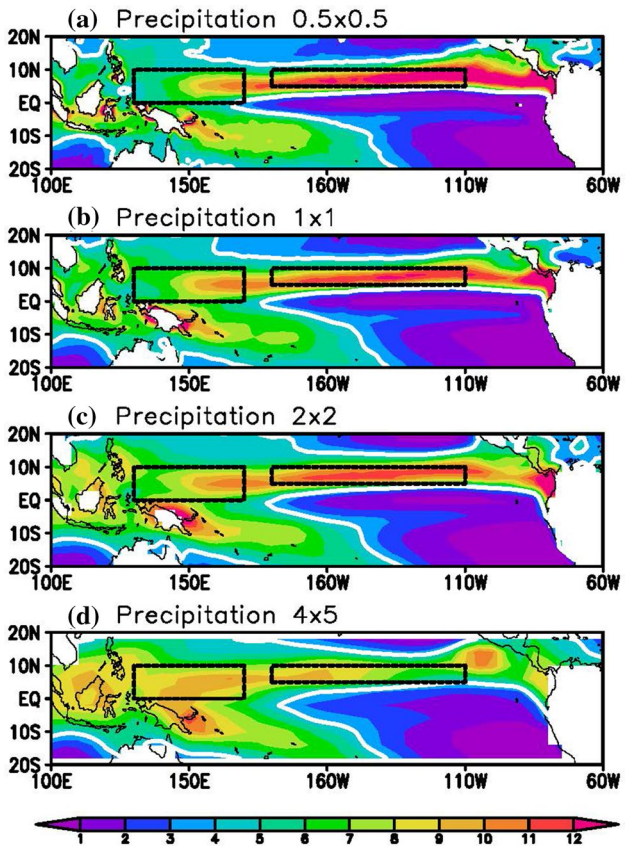

Fig. 5 The spatial distribution of precipitation for four different spatial resolutions. The boxes in each panel are western Pacific (0–10°N, 130–170°E) (left) and eastern Pacific (5–10°N, 180–110°W) (right). The unit is mm day^{-1}

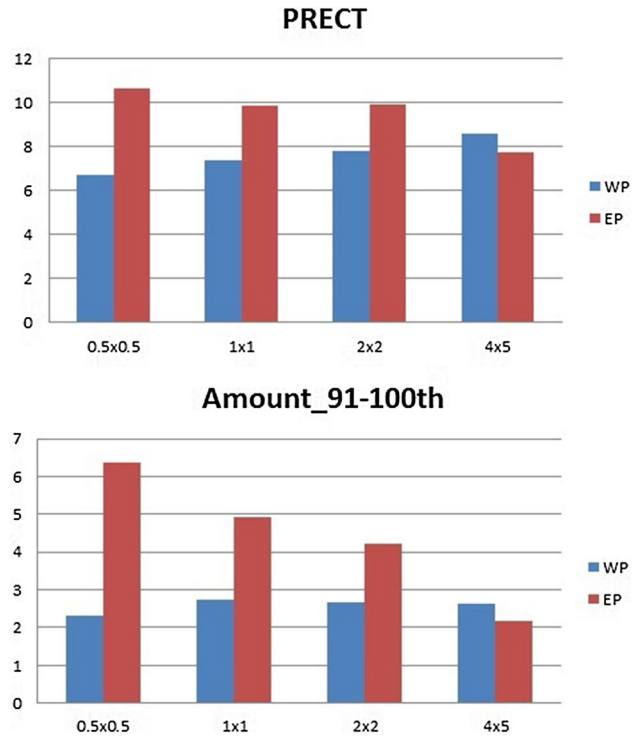

Fig. 6 Precipitation averaged over the boxes in Fig. 5 for western Pacific (blue) and eastern Pacific (red) for **a** the total amount and **b** the amount at the last 10 percentiles bins. The unit is mm day^{-1}

intensity in response to model resolution change in the eastern Pacific ITCZ is an interesting phenomenon that needs to be clarified.

In order to understand why there is a difference between these two domains, we further analyzed the characteristics of tropical precipitation, focusing on the intensity and frequency patterns of the heavy-rain regime (91–100th bins). For the occurrence frequency patterns (Fig. 7), the finer resolution experiment tends to have fewer heavy precipitation events than the coarser one over most of the climatologically ascending regions except over the eastern Pacific where more heavy rain events are observed in the finer resolution runs. For the intensity patterns, the finer resolution experiment, however, tends to generate a stronger precipitation intensity almost everywhere in the tropics (Fig. 8), suggesting that finer resolution experiments are more capable of producing small-scale intense cumulus convection. Overall, the change of total precipitation amount associated with the model spatial resolution seems to be dominated by the precipitation frequency. The precipitation intensity only matters in the eastern Pacific ITCZ for higher resolution runs (1° and 0.5°) (see Figs. 5, 7, 8 for comparison).

Figure 9 shows the domain averages of the precipitation frequency and intensity patterns of the heavy-rain regime (91–100th bins) for different spatial resolution experiments. Over the western Pacific ITCZ, the frequency decreases significantly with the increase of the spatial resolution (Fig. 9a) while the corresponding intensity only increases slightly with the increase of spatial resolution (Fig. 9b), suggesting the dominance of precipitation frequency in determining the precipitation amount (i.e., a weaker magnitude of precipitation over the western Pacific in higher resolution runs shown in Fig. 5). Over the eastern Pacific ITCZ, the frequency of heavy precipitation events in general increases with the increase of spatial model resolution, though the change is marked from 4° to 2° but relatively modest from 2° to 0.5° (Fig. 9a). The precipitation intensity also increases with the increase of model resolution, especially from 1° to 0.5° in determining the precipitation amount. Thus, the higher precipitation amounts in the eastern Pacific in finer resolution experiments appear to come from more frequent occurrences of stronger precipitation events.

To understand what cause more frequent occurrences of stronger precipitation events over the eastern Pacific ITCZ in finer spatial resolution experiments, we again examine the vertical structure of key parameters, as discussed in

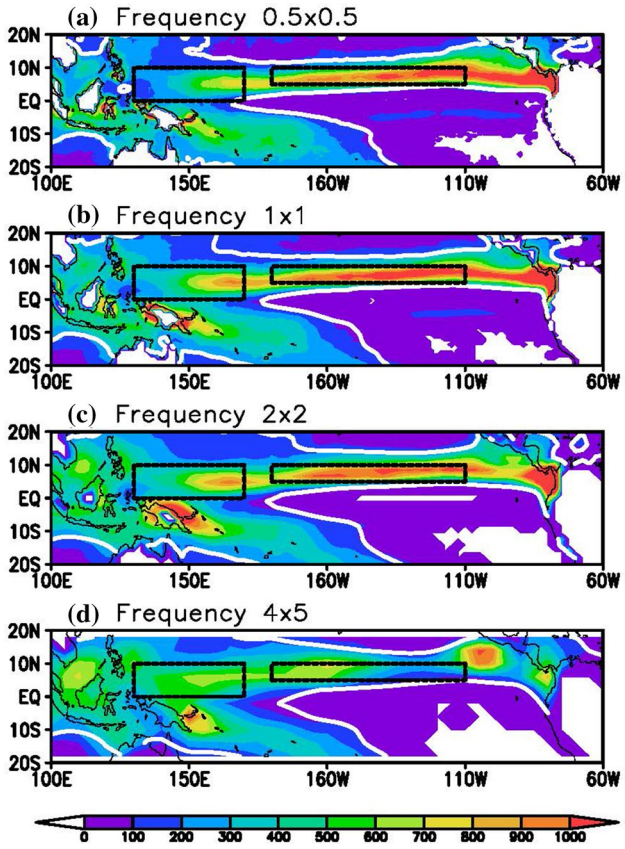

Fig. 7 The spatial distribution of the frequency of precipitation over the last 10 percentiles bins. The unit is number of event

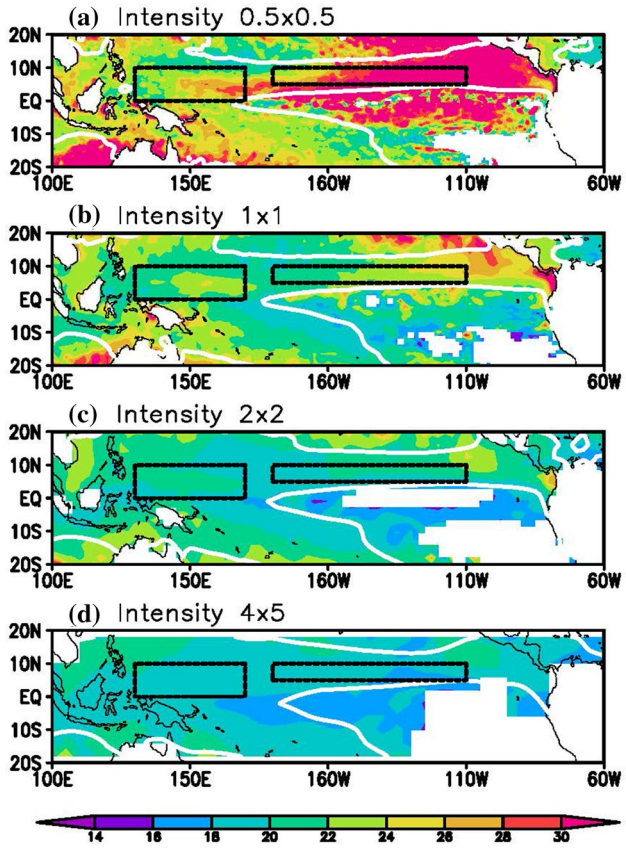

Fig. 8 As in Fig. 7, but for precipitation intensity. The unit is mm day^{-1}

Sect. 4.1. Similar to Fig. 2, we compare the Q_1, Q_2 profiles for the last 10 bins between the western and eastern Pacific ITCZs (Fig. 10). For the Q_1 profile, the top-heavy convection structure shows relatively little dependence on model resolution over the western Pacific ITCZ, except for a slightly greater contribution of bottom-heavy convection in the two finest resolution experiments (Fig. 10a). Over the eastern Pacific ITCZ, the contribution of bottom-heavy convection becomes much greater, while the contribution of top-heavy convection becomes much smaller in the two finest spatial resolution experiments (Fig. 10b). Similar patterns are also observed for Q_2, although the contrast between the western and the eastern Pacific ITCZ is not as clear as in Q_1 (Fig. 10c, d). Note that similar changes are also found for the pressure velocity and divergence fields (not shown). Based on the above findings, we may conclude that a greater contribution of bottom-heavy convection is responsible for more frequent occurrences of heavy precipitation events in the eastern Pacific ITCZ in the finer resolution runs.

5 The moisture budget analysis

In the previous section, we reported the changes in contribution between top-heavy and bottom-heavy convection and the differences in precipitation frequency and intensity tendencies between the western and eastern Pacific ITCZs when the model spatial resolution varies. Here, we employed the moisture budget analysis to explore the possible causes behind such changes. Following Chou and Neelin (2004) and Chou et al. (2009), the vertically integrated moisture equation can been written as

$$P = -\langle \omega \partial_p q \rangle - \langle \mathbf{v} \cdot \nabla q \rangle + E \tag{3}$$

where P is precipitation, E is evaporation (both in W m^{-2}), $\mathbf{v}$ is horizontal wind vector, q is the specific humidity (in energy unit, J kg^{-1}, by absorbing the latent heat per unit mass L). The brackets $\langle\ \rangle$ denotes a mass integration through the troposphere, typically from 1000 hPa to the tropopause. Here, the tropopause level is fixed at 100 hPa as in previous studies (Chen et al. 2016; Bui et al. 2016). In (3), precipitation P is balanced by the vertical moisture advection, $-\langle \omega \partial_p q \rangle$, the horizontal moisture advection, $-\langle \mathbf{v} \cdot \nabla q \rangle$, and the surface evaporation, E.

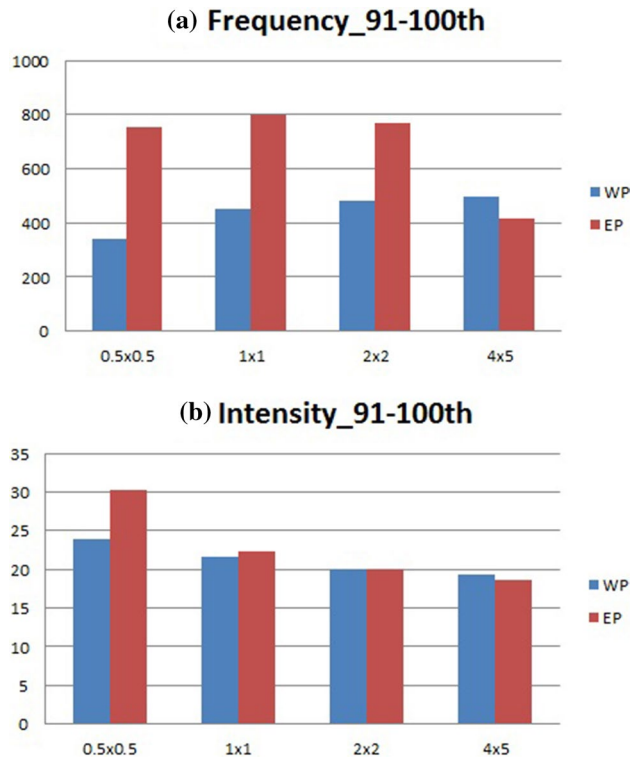

Fig. 9 The **a** frequency and **b** intensity of precipitation over the last 10 percentiles bins for western and eastern Pacific

Figure 11 shows the magnitude of each term in (3) averaged over the two target domains for four different resolutions. It is clear that the vertical moisture advection determines the precipitation amount (comparing the first four groups of column), implying a major balance between drying of precipitation and moistening of vertical moisture transport in convective regions. The contributions from surface evaporation and horizontal moisture advection are small (except in the finest resolution experiment), and the negative value of $-\langle \mathbf{v} \cdot \nabla q \rangle$ implies a horizontal advection of dry air into these regions. Of particular interest shown in Fig. 11 is the reverse tendencies in precipitation and vertical moisture transport terms between the eastern and western Pacific ITCZs. Over the western Pacific ITCZ, both the precipitation and vertical moisture transport terms increase as the model resolution becomes coarser. The situation reverses over the eastern Pacific ITCZ where the precipitation and vertical moisture transport terms increase as the model resolution becomes finer.

As discussed in previous section, there is a marked difference in vertical structure of convection between the western and eastern Pacific ITCZs that could attribute to the above reverse tendencies. To provide a quantitative evaluation of how the vertical structure of convection affects the vertical moisture transport, we decompose vertical moisture transport anomaly into anomaly due to moisture structure change (thermodynamic effect), anomaly due to convective structure and intensity change (dynamic effect of anomalous circulation), and anomaly due to eddy transport of moisture. The prime term is the departure from the corresponding temporal averaged over the tropical mean:

$$-\langle \omega \partial_p q \rangle' = -\langle \overline{\omega} \partial_p q' \rangle - \langle \omega' \partial_p \overline{q} \rangle - \langle \omega' \partial_p q' \rangle \tag{4}$$

As shown, contributions from eddy and thermodynamic effects are relatively small (the sixth and seventh columns in Fig. 11). In contrast, the term due to convection structure and intensity change (dynamic effect) appears to dictate the vertical moisture advection (see the fifth columns in Fig. 11). We also note that the magnitude of the dynamic effect, $\langle \omega' \partial_p \overline{q} \rangle$, decreases as the spatial resolution becomes coarser over the eastern Pacific ITCZ, consistent with the decrease of total precipitation as shown in Fig. 6. In summary, it is the change in convection structure and intensity (i.e., the $\langle \omega' \partial_p \overline{q} \rangle$ term) that determines change of precipitation among different resolutions.

To understand how the convection change affects the vertical moisture transport, we further decompose the pressure velocity ω into a product of its vertical profile and its strength (Yu and Neelin 1997; Chou and Neelin 2004; Chou et al. 2013; Chen et al. 2016):

$$\omega = -\Omega(p) \nabla \cdot \mathbf{v}_T(x, y) \tag{5}$$

where $\Omega(p)$ describes the vertical structure of vertical velocity (convection), and $\nabla \cdot \mathbf{v}_T$ is the divergence induced by the first baroclinic winds, representing the intensity of vertical velocity (convection) and a positive $\nabla \cdot \mathbf{v}_T$ denotes upward motion. In this study, Ω is estimated from ω by a normalization using the vertical integral of its corresponding intensity at each level, i.e., $\Omega(p) = \frac{\omega}{\sqrt{\sum_{P_S}^{P_T} \omega^2}}$, similar to Chen et al. (2016). Therefore, the second term on the right hand side of (4) can be written as

$$-\langle \omega' \partial_p \overline{q} \rangle = \langle \nabla \cdot \mathbf{v}_T' \overline{\Omega} \partial_p \overline{q} \rangle + \langle \nabla \cdot \overline{\mathbf{v}_\mathbf{T}} \Omega' \partial_p \overline{q} \rangle \tag{6}$$

Comparing the last two columns in Fig. 11, the contribution of $\langle \nabla \cdot \mathbf{v}_T' \overline{\Omega} \partial_p \overline{q} \rangle$ is relatively small in both regions. It is the change in vertical velocity profile, i.e., $\langle \nabla \cdot \overline{\mathbf{v}_\mathbf{T}} \Omega' \partial_p \overline{q} \rangle$, that accounts for $-\langle \omega' \partial_p \overline{q} \rangle$. One should note that this vertical structure of convection is very sensitive to the spatial resolution used in climate model (as shown in Sect. 4.1). The above results confirm that the differences in precipitation tendencies between the western and eastern Pacific ITCZs among various spatial resolution experiments shown in Sect. 4.2 are determined mainly by changes in total precipitation contribution between the top-heavy and bottom-heavy convection (i.e., changes in the vertical structure of convection).

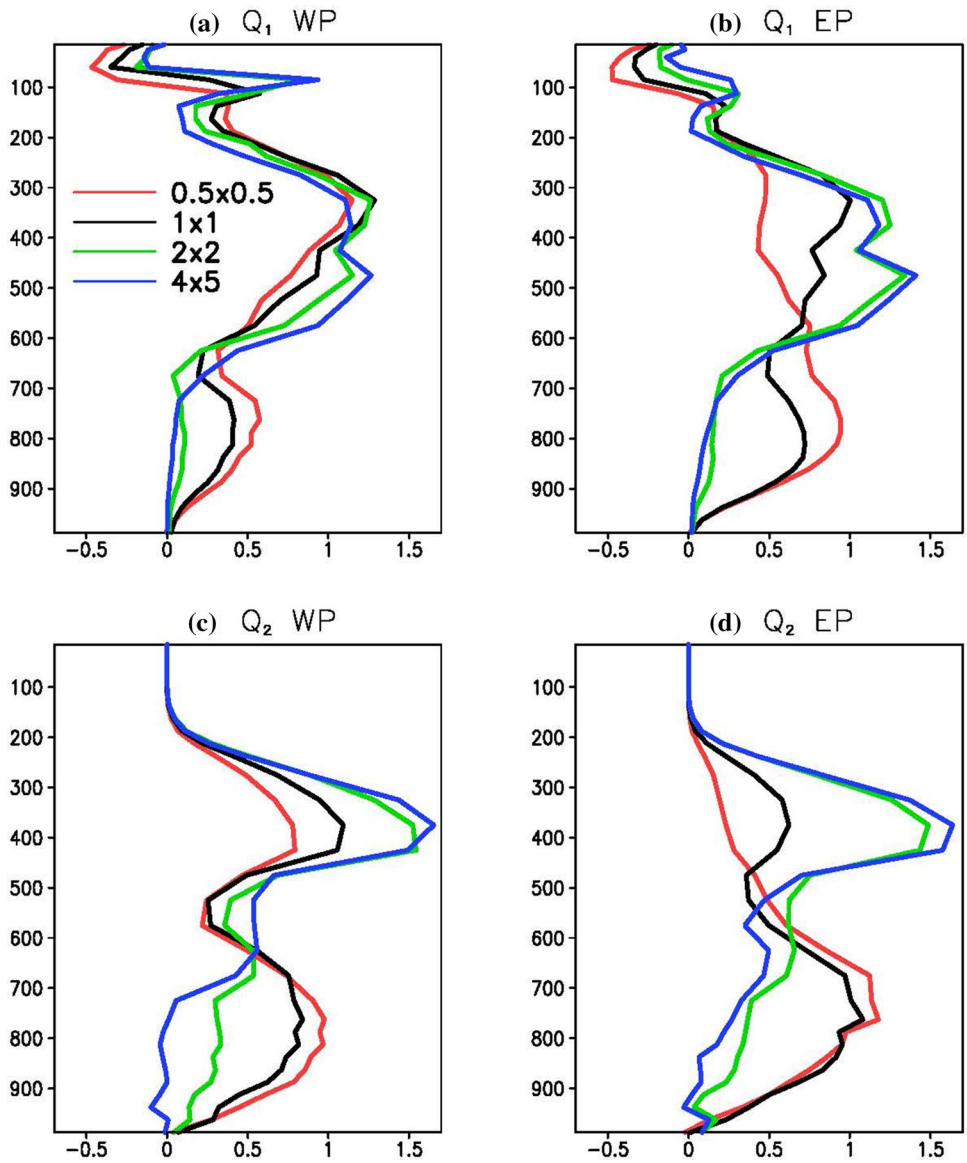

Fig. 10 The vertical structure of **a**, **b** Q_1 and **c**, **d** Q_2 for the last 10 percentiles bins of four different spatial resolutions. **a** and **c** are averaged over western Pacific; **b** and **d** are averaged over eastern Pacific

6 Summary and discussion

This paper examines how the model spatial resolution impacts simulations of tropical climate, with a focus on the vertical structure of convection. We analyze the vertical profiles of apparent heat source (Q_1) and moisture sink (Q_2) at the first and last 10 percentiles of precipitation events, representing respectively the light- and heavy-rain regimes. We also compare the differences in precipitation behaviors between the western and eastern Pacific ITCZs dominated climatologically by top-heavy and bottom-heavy convection, respectively. Some notable findings are summarized as follow:

(1) Contributions to the total precipitation from top-heavy and bottom-heavy convection are sensitive to model's spatial resolution, especially in the heavy-rain regime (91–100th percentiles). A greater contribution from bottom-heavy convection and less contribution from top-heavy convection are found in the finer resolution experiments (Fig. 2).

(2) From the regional point of view, coarser resolution experiments exhibit stronger precipitation in the western Pacific warm pool, but weaker precipitation in the eastern Pacific ITCZ (see Figs. 5, 6). In the former region where the convective structure is dominated by top-heavy convection, precipitation increases in coarser resolution experiments are due to higher occurrence frequencies of heavy rainfall (last 10 bins) events associated with a warmer environment. In the latter region, the heavy precipitation events are dominated by bottom-heavy structure of convection in the higher

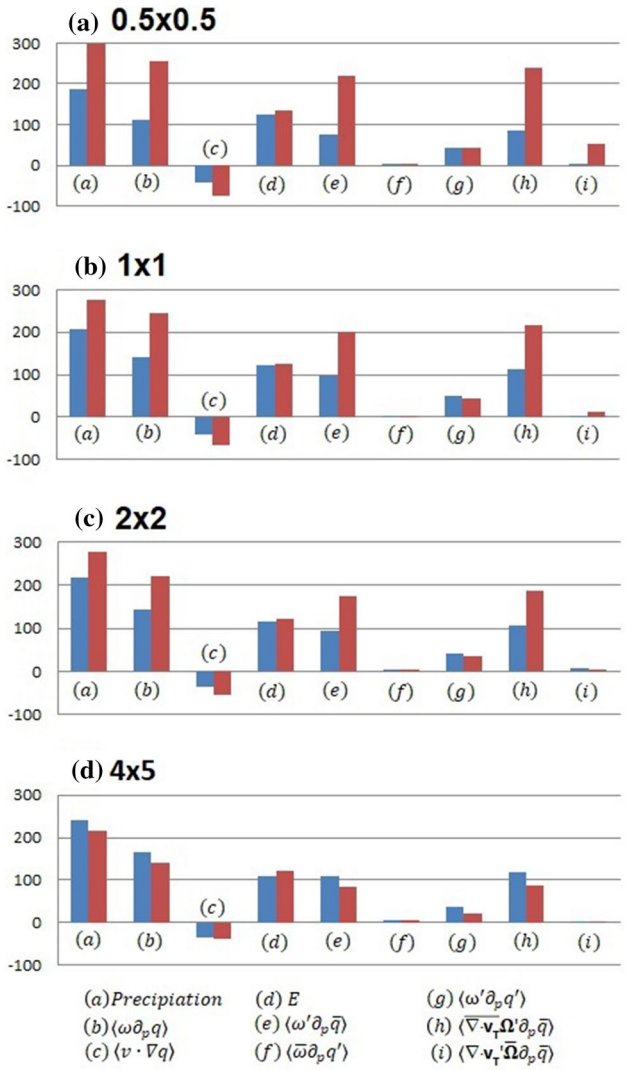

Fig. 11 Magnitude of each moisture budget terms and its decomposition: the first four, **a**–**d**, are from Eq. 3, the next three (**e**, **f**, **g**) are from Eq. 4, and the last two (**h**, **i**) are from Eq. 6, averaged over the western (blue) and eastern (red) Pacific ITCZs for different spatial resolutions. The unit is W m^{-2}

resolution simulation, and this leads to more frequent occurrence of heavy rainfall events and therefore more precipitation (see Figs. 9, 10).

(3) The moisture budget analysis (see Fig. 11) further suggests that, in the heavy-rain regime, the differences in precipitation tendencies between the western and eastern Pacific ITCZs among various spatial resolution experiments (Sect. 4.2) are determined mainly by changes in convective structure (i.e., the shape of convection) rather than changes in convective strength. More contribution from bottom-heavy structure of convection occurs in the finer resolution; while more contribution from top-heavy structure of convection tends to occur in the coarser resolution experiments, which is particularly evident in the eastern Pacific ITCZ (Sect. 4.2).

This study for the first time shows the sensitivity of model's spatial resolution in determining the contribution between top-heavy convection and bottom-heavy convection in tropical climate. A recent study by Bui et al. (2016) indicated that the very different results of the vertical transport of moist static energy (MSE) between the western and eastern Pacific ITCZs (e.g., positive column-integrated vertical MSE transport in the western Pacific and negative column-integrated vertical MSE transport in the eastern Pacific) should come from different shapes of vertical motion in these two regions. A top-heavy (bottom-heavy) structure of vertical motion, such as the case happening in the western (eastern) Pacific ITCZ, favors a positive (negative) value of MSE transport.

Although the stratiform precipitation may have a significant contribution to the total precipitation (Xu 2009; Johnson et al. 2016), however, it seems impossible to separate the convective and stratiform preciptiation in this study as a clear quantitative separation requires high-resolution observations (e.g., meteorological radar) or non-hydrostatic mesoscale numerical simulations [e.g., WRF or CRM (cloud resolving model)]. This is beyond the scope of this study and we prefer to put it in our future work.

Finally, one major concern arising from this study broaches the question of whether there is a minimum spatial resolution for climate models in order to reproduce a reasonable climatology of the structure of tropical convection (or large-scale vertical motions from the sense of model simulations). The results presented here suggest that a spatial resolution finer than $2° \times 2°$ is required for climate models to obtain a reasonable precipitation contribution between top-heavy and bottom-heavy convection, especially in the eastern Pacific, along with a fair convective adjustment process associated with the vertical MSE transport in the tropical ITCZs.

Acknowledgements This research is supported by the Ministry of Science and Technology (MOST) in Taiwan under Grants NSC102-2111-M-001-002-MY3, MOST104-2111-M-008-026-MY2, and MOST105-2111-M-008-025-MY3. The first author (HX Bui) thanks Dr. Wei-Liang Lee for useful discussions. The authors also acknowledge the two anonymous reviewers for their appreciation to our work and many constructive comments to improve the quality of this manuscript.

References

Back LE, Bretherton CS (2006) Geographic variability in the export of moist static energy and vertical motion profiles in the tropical Pacific. Geophy Res Lett 33(17)

Boyle J, Klein SA (2010) Impact of horizontal resolution on climate model forecasts of tropical precipitation and diabatic heating for the TWP-ICE period. J Geophys Res 115(D23)

Bretherton CS, McCaa JR, Grenier H (2004) A new parameterization for shallow cumulus convection and its application to marine subtropical cloud-topped boundary layers. Part I: Description and 1D results. Mon Weather Rev 132(4):864–882

Bretherton CS, Park S (2009) A new moist turbulence parameterization in the community atmosphere model. J Clim 22(12):3422–3448

Bui HX, Yu J-Y, Chou C (2016) Impacts of vertical structure of large-scale vertical motion in tropical climate: Moist static energy framework. J Atmos Sci 73(11):4427–4437

Chan SC, Nigam S (2009) Residual diagnosis of diabatic heating from ERA-40 and NCEP reanalyses: intercomparisons with TRMM. J Clim 22(2):414–428

Chen C-A, Yu J-Y, Chou C (2016) Impacts of vertical structure of convection in global warming: the role of shallow convection. J Clim 29(12):4665–4684

Chou C, Chen C-A, Tan P-H, Chen KT (2012) Mechanisms for global warming impacts on precipitation frequency and intensity. J Clim 25(9):3291–3306

Chou C, Neelin JD (2004) Mechanisms of global warming impacts on regional tropical precipitation*. J Clim 17(13):2688–2701

Chou C, Neelin JD, Chen C-A, Tu J-Y (2009) Evaluating the "rich-get-richer" mechanism in tropical precipitation change under global warming. J Clim 22(8):1982–2005

Chou C, Wu T-C, Tan P-H (2013) Changes in gross moist stability in the tropics under global warming. Clim Dyn 41(9–10):2481–2496

Deser C, Capotondi A, Saravanan R, Phillips AS (2006) Tropical Pacific and Atlantic climate variability in CCSM3. J Clim 19(11):2451–2481

Gregory D, Kershaw R, Inness PM (1997) Parametrization of momentum transport by convection. II: Tests in single-column and general circulation models. Q J R Meteorol Soc 123(541):1153–1183

Hack JJ, Caron JM, Danabasoglu G, Oleson KW, Bitz C, Truesdale JE (2006) CCSM-CAM3 climate simulation sensitivity to changes in horizontal resolution. J Clim 19(11):2267–2289

Hagos S et al (2010) Estimates of tropical diabatic heating profiles: commonalities and uncertainties. J Clim 23(3):542–558

Held IM, Soden BJ (2006) Robust responses of the hydrological cycle to global warming. J Clim 19(21):5686–5699

Holloway CE, Neelin JD (2007) The convective cold top and quasi-equilibrium*. J Atmos Sci 64(5):1467–1487

Houze RA (1997) Stratiform precipitation in regions of convection: a meteorological paradox? Bull Am Meteorol Soc 78:21792196

Johnson RH, Rickenbach TM, Rutledge SA, Ciesielski PE, Schubert WH (1999) Trimodal characteristics of tropical convection. J Clim 12(8):2397–2418

Johnson RH, Ciesielski PE, Rickenbach TM (2016) A further look at Q1 and Q2 from TOGA COARE. Meteorol Monogr 56:1.1–1.12

Kain JS, Fritsch JM (1990) A one-dimensional entraining/detraining plume model and its application in convective parameterization. J Atmos Sci 47(23):2784–2802

Lau KM et al (2000) A report of the field operations and early results of the south china sea monsoon experiment (SCSMEX). Bull Am Meteorol Soc 81(6):1261–1270

Lin S-J (2004) A vertically lagrangian finite-volume dynamical core for global models. Mon Weather Rev 132(10):2293–2307

Ling J, Zhang C (2013) Diabatic heating profiles in recent global reanalyses. J Clim 26(10):3307–3325

Neale RB, Richter JH, Jochum M (2008) The impact of convection on ENSO: from a delayed oscillator to a series of events. J Clim 21(22):5904–5924

Neale RB et al (2010) Description of the NCAR community atmosphere model (CAM 5.0). NCAR Tech. Note NCAR/TN-486+ STR

Neelin JD (2007) Moist dynamics of tropical convection zones in monsoons, teleconnections and global warming, Chap. 10, 400. Princeton University Press

Nigam S, Chung C, DeWeaver E (2000) ENSO diabatic heating in ECMWF and NCEP-NCAR reanalyses, and NCAR CCM3 simulation. J Clim 13(17):3152–3171

Park S, Bretherton CS (2009) The university of Washington shallow convection and moist turbulence schemes and their impact on climate simulations with the community atmosphere model. J Clim 22(12):3449–3469

Richter JH, Rasch PJ (2008) Effects of convective momentum transport on the atmospheric circulation in the community atmosphere model, version 3. J Clim 21(7):1487–1499

Schumacher C, Zhang MH, Ciesielski PE (2007) Heating structures of the TRMM field campaigns. J Atmos Sci 64(7):2593–2610

Sobel AH, Yuter SE, Bretherton CS, Kiladis GN (2004) Large-scale meteorology and deep convection during TRMM KWAJEX*. Mon Weather Rev 132(2):422–444

Stephens GL et al (2010) Dreary state of precipitation in global models. J Geophys Res 115(D24)

Stokes GM, Schwartz SE (1994) The atmospheric radiation measurement(ARM) program: programmatic background and design of the cloud and radiation test bed. Bull Am Meteor Soc 75(7):1201–1221

Sun Y, Solomon S, Dai A, Portmann RW (2007) How often will it rain? J Clim 20(19):4801–4818

Takayabu YN, Shige S, Tao W-K, Hirota N (2010) Shallow and deep latent heating modes over tropical oceans observed with TRMM PR spectral latent heating data. J Clim 23(8):2030–2046

Tao W-K et al (2006) Retrieval of latent heating from TRMM measurements. Bull Am Meteorol Soc 87(11):1555–1572

Webster PJ, Lukas R (1992) TOGA COARE: the coupled ocean-atmosphere response experiment. Bull Am Meteorol Soc 73(9):1377–1416

Xie S, Hume T, Jakob C, Klein SA, McCoy RB, Zhang M (2010) Observed large-scale structures and diabatic heating and drying profiles during TWP-ICE. J Clim 23(1):57–79

Xu K (2009) Partitioning mass, heat, and moisture budgets of explicitly simulated cumulus ensembles into convective and stratiform components. J Atmos Sci 52:551573

Yanai M, Esbensen S, Chu J-H (1973) Determination of bulk properties of tropical cloud clusters from large-scale heat and moisture budgets. J Atmos Sci 30(4):611–627

Yanai M, Johnson R (1993) Impacts of cumulus convection on thermodynamic fields. 39–62

Yu J-Y, Neelin JD (1997) Analytic approximations for moist convectively adjusted regions. J Atmos Sci 54(8):1054–1063

Zhang G, McFarlane NA (1995) Sensitivity of climate simulations to the parameterization of cumulus convection in the Canadian climate centre general circulation model. Atmo Ocean 33(3):407–446